Computers and Mathematics with Applications 75 (2018) 1868–1881

Contents lists available at ScienceDirect

Computers and Mathematics with Applications

journal homepage: www.elsevier.com/locate/camwa

Higher degree immersed finite element spaces constructed according to the actual interface

Slimane Adjerid [a], Mohamed Ben-Romdhane [b], Tao Lin [a,*]

[a] Department of Mathematics, Virginia Tech, Blacksburg, VA 24061, USA
[b] Department of Mathematics and Natural Sciences, Gulf University for Science and Technology, Mishref, Kuwait

ARTICLE INFO

Article history:
Available online 16 November 2017

Keywords:
Interface problems
Immersed finite element method
Cartesian mesh
Structured mesh
Higher order finite element methods

ABSTRACT

We discuss the construction of higher degree immersed finite element (IFE) spaces that can be used to solve two dimensional second order elliptic interface problems having general interfaces without requiring the mesh to be aligned with the material interfaces. The optimal approximation capability of the proposed piecewise pth degree IFE spaces are demonstrated by numerical experiments with interpolations. Numerical solutions to interface problems generated from a partially penalized method based on the proposed higher order IFE spaces also suggest optimal convergence in both the L^2 and H^1 norms under mesh refinement.

1. Introduction

In this article we report our recent explorations about constructing higher degree immersed finite element (IFE) spaces for solving elliptic interface problems. To be specific and without loss of generality, we consider a bounded domain $\Omega \subset \mathbb{R}^2$ that is separated into two subsets Ω^+ and Ω^- by a curve Γ, see Fig. 1.1. In this domain, we consider the following typical second order elliptic interface problem

$$\begin{cases} -\nabla \cdot (\beta \nabla u) = f, & \text{on } \Omega^- \cup \Omega^+, \\ u_{|\partial\Omega} = g, & \text{on } \partial\Omega, \end{cases} \tag{1.1}$$

with

$$\beta = \begin{cases} \beta^-, & \text{in } \Omega^-, \\ \beta^+, & \text{in } \Omega^+ \end{cases}$$

where $\min(\beta^-, \beta^+) > 0$. The exact solution of this model elliptic problem satisfies the following interface jump conditions

$$[u]_\Gamma = 0, \tag{1.2a}$$

$$[\beta\, \boldsymbol{n} \cdot \nabla u]_\Gamma = 0. \tag{1.2b}$$

We also note that when the right-hand side of the elliptic problem is in C^{p-2}, then

$$[\beta \frac{\partial^l \Delta u}{\partial \boldsymbol{n}^l}]_\Gamma = 0, \quad l = 0, 1, \ldots, p-2. \tag{1.2c}$$

* Corresponding author.
E-mail address: tlin@vt.edu (T. Lin).

https://doi.org/10.1016/j.camwa.2017.10.010
0898-1221/

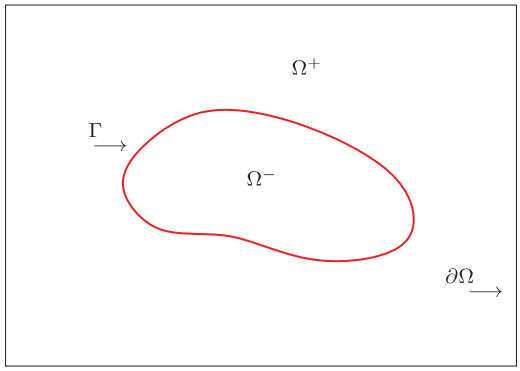

Fig. 1.1. A two-material solution domain Ω.

where the jump $[v]_\Gamma = v^+|_\Gamma - v^-|_\Gamma$ with $v^\pm = v|_{\Omega^\pm}$. The conditions (1.2a) and (1.2b) are called the physical jump conditions while the jump equations (1.2c) are suggested by the smoothness of the right-hand side in (1.1).

Generally speaking, a standard finite element method based on generic problem-independent polynomial shape functions should not have much difficulty, if any, to produce an accurate numerical approximation to the exact solution of the interface problem described by (1.1), (1.2a), and (1.2b) provided that its mesh is "body-fitted" meaning the mesh is formed according to the interface Γ such that each element of this mesh is essentially on one side of Γ. It is well-known [1–3] that, without a "body-fitted" mesh, there is generally no guarantee that the approximate solution produced by a standard finite element method can converge optimally, if it converges at all. This "body-fitted" requirement can hinder applications of standard finite element methods to simulations in which an interface problem has to be repeatedly solved with different interface configurations because it demands a new mesh to be made for each new interface.

On the other hand, immersed finite element (IFE) methods are developed to solve interface problems with interface independent meshes [4–19]. Most elements in the mesh used by an IFE method have no intersection with the interface where generic problem independent polynomial shape functions can still be used as usual. On interface elements, i.e., those elements cut by the interface Γ, an IFE method relies on problem-dependent shape functions constructed according to the jump conditions specified by the interface problem. The problem-dependent shape functions are macro elements, similar to the well-known Hsieh–Clough–Tocher elements [20,21], which are piecewise polynomials patched together by jump conditions. This idea traces back to the generalized finite element method which appeared in 1970s [22,23] and employed shape functions on an element constructed by locally solving the problem in that element, these shape functions may be non-polynomials and were capable of capturing important features of the exact solution.

Since there have been quite a few publications on lower degree (using polynomials of degree 1 or less) IFE methods, developing higher degree IFE spaces is not only the natural next step but also desirable because they can be useful in modern techniques such as the local h and p refinement. Works for one dimensional IFE spaces can be found in [4,6,8,24] while some exploratory work for two dimensional IFE space are in [5,7]. These preliminary works lead us to two essential issues in developing higher degree IFE space. The first issue is a need for extra conditions for determining coefficients of the higher degree polynomials in a higher degree IFE shape function. We note that the physical jump conditions given in an interface problem can be naturally used to uniquely determine a lower degree IFE shape function [10,12,14,15,17], but they are not enough for an IFE shape function constructed with higher degree polynomials. We will show how extended jump conditions such as those given (1.2c) can be employed to augment the given physical jump conditions for constructing higher degree IFE spaces while other types of extended jump conditions are possible [5,7].

The second issue is the interface for IFE functions and how to impose jump conditions on it. For IFE functions constructed by linear or bilinear polynomials, each interface element is partitioned into two sub-elements by a line or a plane approximating the interface Γ and IFE functions on this element are piecewise linear or bilinear polynomial according to these two sub-elements with straight edges. This means the interface of a linear or bilinear IFE function is a polyline across which the jump conditions are naturally applied. While a polyline can approximate a curve interface Γ with $O(h^2)$ accuracy expected from linear or bilinear polynomial, it is not enough to match the desired $O(h^{p+1})$ accuracy when pth degree polynomial is used for IFE functions with $p > 1$. In this article, we propose IFE functions constructed according to the actual interface Γ, not its approximation, and we propose to enforce the interface jump conditions (including those extended ones) by projection to pertinent polynomials spaces through integrals over the interface; hence, the higher degree IFE spaces developed in this article can be applied to more realistic interface problems while those explored in [5,7] can only be employed in special situations such that the interface in each interface element is a strait line.

Essentially, the IFE spaces proposed here are more sophisticated than those in the literature made with lower degree polynomials. It is known, see [10,15] for example, the error estimation even for lower degree IFE spaces demands special complicated techniques because of inapplicability of the powerful scaling argument for standard finite element error

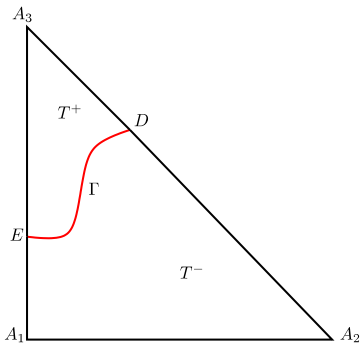

Fig. 2.1. An interface element.

analysis; therefore, our focus here is the systematic construction of higher degree IFE spaces and the related error analysis is tacitly considered as an important and challenging research topic in the next step. We note that, by the proposed construction, the pieces of a higher degree IFE function are stitched together in each interface element across the actual interface Γ by imposing the interface jump conditions (including those extended ones given in (1.2c)) only in a weak sense, and this might be just one of major difficulties in the related error estimation. Nevertheless, our extensive numerical experiments, some of them are reported here in Section 4, suggest that the proposed higher degree IFE spaces can perform optimally.

This article consists of the following sections. In Section 2, we discuss the construction of both Lagrange type and hierarchical type pth degree IFE shape functions on interface elements. Section 3 discusses some implementation issues for using higher degree IFE spaces, such as suitable numerical quadrature and finite element schemes. Section 4 presents numerical results for demonstrating the optimal convergence of the proposed pth degree IFE spaces. Section 5 provides a few conclusions.

2. Higher degree IFE spaces and shape functions

Let $\mathcal{T}_h$ be a triangular mesh of the solution domain Ω and let $\mathcal{E}_h$ be the set of all the edges of this mesh. We shall refer to elements (resp. edges) cut by the interface as interface elements (resp. interface edges), and denote the set of interface elements (edges) by $\mathcal{T}_h^i$ (resp. $\mathcal{E}_h^i$). We will also use $\mathcal{T}_h^n = \mathcal{T}_h \setminus \mathcal{T}_h^i$ and $\mathcal{E}_h^n = \mathcal{E}_h \setminus \mathcal{E}_h^i$ to denote the sets of non-interface elements and the set of non-interface edges, respectively. Without loss of generality we assume that the interface Γ is defined by the parametric equations $x = x(t)$ and $y = y(t)$ for $0 \le t \le 1$. Our goal here is to develop the pth degree ($p \ge 1$ is an integer) IFE space for solving the typical elliptic interface problem (1.1)-(1.2b). Since an IFE space will use the standard finite element functions on all non-interface elements, we focus on constructing pth degree IFE functions on interface elements.

Let $T \in \mathcal{T}_h^i$ be a typical interface element and assume $T \cap \Gamma$, the restriction of interface Γ to element T, is described by $(x(t), y(t))$ for $0 \le t_0 \le t \le t_1 \le 1$. The curve $T \cap \Gamma$ meets the edges of T at points D and E and it naturally partitions T into two sub-elements T^- and T^+ such that T^- and T^+ contain vertices of T in Ω^- and Ω^+, respectively, see the illustration Fig. 2.1. The pth degree IFE functions to be constructed on the interface element T is in the following piecewise form:

$$\varphi(x, y) = \begin{cases} \varphi^-(x, y) \in \mathcal{P}_p, & (x, y) \in T^-, \\ \varphi^+(x, y) \in \mathcal{P}_p, & (x, y) \in T^+, \end{cases} \tag{2.1}$$

where $\mathcal{P}_p$ is the space of polynomials with degree p or less.

Coefficients in the p-degree polynomials φ^- and φ^+ of a pth degree IFE function are to be determined such that φ can satisfy interface jump conditions (1.2a) and (1.2b), if possible. However, the restriction of a polynomial to a general interface curve Γ is not necessarily a polynomial. Hence, because of its limited degree of freedom, a pth degree IFE function defined by (2.1) usually cannot satisfy the interface jump conditions (1.2a) and (1.2b) on the interface curve Γ except for those with extremely simple geometries. Therefore, instead of requiring φ^- and φ^+ to satisfy the jump conditions on Γ precisely, we propose to make them to satisfy the jump conditions in a weak sense such that their jumps across the interface are orthogonal to pertinent polynomials spaces.

To be specific, we let

$$\mathcal{P}_p(T \cap \Gamma) = Span\{t^i, i = 0, 1, 2, \ldots, p\},$$

and for two functions $v(t)$ and $w(t)$ mapping $[t_0, t_1]$ to $\mathbb{R}$, we denote

$$\langle v, w \rangle_{T\cap\Gamma} = \int_{T\cap\Gamma} v(t)w(t)dt.$$

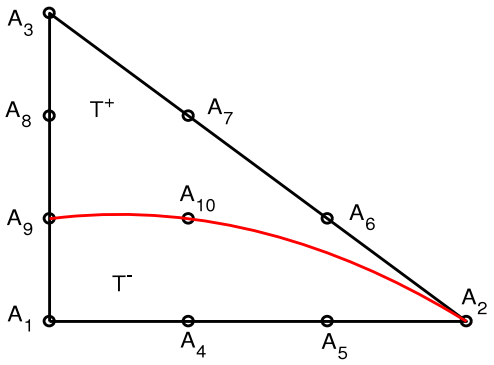

Fig. 2.2. An interface element and related partition of node indices.

For a function $v(x, y)$, its restriction on Γ is $v(x(t), y(t))$ and its inner product with $w(t) \in \mathcal{P}_p(T \cap \Gamma)$ on $T \cap \Gamma$ is understood accordingly.

When the interface $T \cap \Gamma$ has the simplest geometry, i.e. $T \cap \Gamma$ is a straight line, the restrictions of $[\varphi]$ and $[\beta\, \boldsymbol{n} \cdot \nabla\varphi]$ to the line segment $T \cap \Gamma$ are polynomials of degree p and $p-1$, respectively. Hence, for a general curve $T \cap \Gamma$, the interface jump conditions (1.2a) and (1.2b) suggest to require a pth degree IFE function φ in the form of (2.1) to satisfy the following conditions:

$$\langle [\varphi], w \rangle_{T\cap\Gamma} = 0, \ \forall w \in \mathcal{P}_p(T \cap \Gamma) \tag{2.2a}$$

$$\langle [\beta\, \boldsymbol{n} \cdot \nabla\varphi], w \rangle_{T\cap\Gamma} = 0, \ \forall w \in \mathcal{P}_{p-1}(T \cap \Gamma). \tag{2.2b}$$

In addition, the extended jump conditions in (1.2c) lead to the following conditions for pth degree IFE functions:

$$\langle [\beta \frac{\partial^l \Delta\varphi}{\partial \boldsymbol{n}^l}], w \rangle_{T\cap\Gamma} = 0, \ l = 0, 1, \ldots, p-2, \ \forall w \in \mathcal{P}_{p-2-l}. \tag{2.2c}$$

Therefore, the local pth-degree IFE space to be constructed on an interface element $T \in \mathcal{T}_h^i$ will be in the following form:

$$\mathcal{S}_h^{(p)}(T) = \{\varphi, \ | \ \varphi \text{ satisfies (2.1) and (2.2)}\}. \tag{2.3}$$

Note that a pth degree piecewise polynomial in the form of (2.1) had $(p+1)(p+2)$ coefficients. The interface jump conditions (2.2a)–(2.2c) provide $\frac{1}{2}(p+1)(p+2)$ constraints. Therefore, the degree of freedom for each function in $\mathcal{S}_h^{(p)}(T)$ should be $\frac{1}{2}(p+1)(p+2)$, and we naturally expect

$$dim(\mathcal{S}_h^{(p)}(T)) = dim(\mathcal{P}_p) = \frac{1}{2}(p+1)(p+2)$$

which is consistent with the local IFE spaces on every non-interface element $T \in \mathcal{T}_h^n$ where the standard pth degree polynomial space $\mathcal{P}_p$ is employed. In the next two subsections, we will present two procedures for constructing $\frac{1}{2}(p+1)(p+2)$ shape functions for the local IFE space $\mathcal{S}_h^{(p)}(T)$.

2.1. Lagrange type IFE shape functions

As usual, on each element $T \in \mathcal{T}_h$, we introduce $dim(\mathcal{P}_p)$ nodes $A_i, \ i = 1, 2, \ldots, dim(\mathcal{P}_p)$ and the associated standard Lagrange shape functions $L_i^{(p)}, \ i = 1, 2, \ldots, dim(\mathcal{P}_p)$. On an interface element $T \in \mathcal{T}_h^i$, let $\mathscr{I}$ be the set of node indices. The interface Γ and sub-element T^- and T^+ will partition $\mathscr{I}$ into $\mathscr{I}^+$, $\mathscr{I}^-$ and $\mathscr{I}^0$, respectively, which are the sets of indices for nodes in T^+, in T^-, and on the interface $T \cap \Gamma$. Fig. 2.2 provides an illustration for this partition for the 3-rd degree IFE functions where $\mathscr{I}^+ = \{3, 6, 7, 8\}$, $\mathscr{I}^- = \{1, 4, 5\}$ and $\mathscr{I}^0 = \{2, 9, 10\}$.

Then, we define the Lagrange type pth degree IFE shape function associated with the ith node to be the IFE function $\varphi_i^{(p)} \in \mathcal{S}_h^{(p)}(T)$ such that

$$\varphi_i^{(p)}(A_j) = \delta_{ij}, \ i, j = 1, 2, \ldots, dim(\mathcal{P}_p). \tag{2.4}$$

Table 2.1
Condition numbers for the IFE shape functions with fixed $\beta^- = 1$.

β^+	$a = 0.9$	$a = 0.99$	$a = 0.999$	$a = 0.9999$	$a = 0.99999$	$a = 0.999999$
10	1.121e+3	7.749e+3	7.341e+4	7.304e+5	7.301e+6	7.301e+7
100	1.618e+4	1.174e+5	7.847e+5	7.343e+6	7.297e+7	7.292e+8
500	8.518e+4	7.818e+5	5.011e+6	3.782e+7	3.659e+8	3.647e+9
1000	1.715e+5	1.654e+6	1.181e+7	7.858e+7	7.344e+8	7.297e+9

Using the index partition $\mathscr{I}^+$, $\mathscr{I}^-$ and $\mathscr{I}^0$, we can easily see that the nodal value constraints in (2.4) suggest to construct the pth-degree Lagrange type IFE shape function $\varphi_i^{(p)}$, $i \in \mathscr{I}$ in the following form:

$$\varphi_i^{(p)}(x,y) = \begin{cases} \varphi_i^{(p),+}(x,y) \\ \varphi_i^{(p),-}(x,y) \end{cases} = L_i^{(p)}(x,y) + \begin{cases} \sum_{j\in\mathscr{I}^-} c_j^{(i)} L_j^{(p)}(x,y) & \text{on } T^+, \\ \sum_{j\in\mathscr{I}^+} c_j^{(i)} L_j^{(p)}(x,y) & \text{on } T^-, \end{cases} \tag{2.5}$$

where the coefficients $c_j^{(i)}$, $j = 1, 2, \ldots, |\mathscr{I}^+| + |\mathscr{I}^-|$ are to be determined by enforcing the jump conditions (2.2).

For instance, on the cubic interface element of Fig. 2.2 we use the standard Lagrange cubic shape functions $L_i^{(3)}$, $i = 1, 2, \ldots, 10$ to write the cubic IFE shape functions $\varphi_i^{(3)}$ for all vertices $i = 1, 2, \ldots, 10$ including the ones on the interface as

$$\begin{aligned} &\varphi_i^{(3)}(x,y) = L_i^{(3)}(x,y) + \tilde{\varphi}_i^{(3)}(x,y), \\ &\tilde{\varphi}_i^{(3)}(x,y) = \begin{cases} c_1^{(i)} L_1^{(3)}(x,y) + c_4^{(i)} L_4^{(3)}(x,y) + c_5^{(i)} L_5^{(3)}(x,y) & \text{on } T^+ \\ c_3^{(i)} L_3^{(3)}(x,y) + c_6^{(i)} L_6^{(3)}(x,y) + c_7^{(i)} L_7^{(3)}(x,y) + c_8^{(i)} L_8^{(3)}(x,y) & \text{on } T^-. \end{cases} \end{aligned} \tag{2.6}$$

Since each $\varphi_i^{(3)}$ is continuous at the interface vertices A_2, A_9, A_{10}, we determine its coefficients $c_1^{(i)}$, $c_3^{(i)}$, $c_4^{(i)}$, $c_5^{(i)}$, $c_6^{(i)}$, $c_7^{(i)}$, $c_8^{(i)}$ by enforcing (2.2a) with $w = 1$, (2.2b) and (2.2c). Other interface-nodes configurations can be handled similarly, and the resulting algebraic system can be used to solve for the coefficients in a shape function. However, this algebraic system might become ill conditioned if one or more nodes are close to but not on the interface as illustrated by data in Table 2.1 for the cubic IFE shape functions on the element with vertices (0, 0), (0, 1), and (1, 1) cut by the vertical interfaces $x = a$, $a = 0.9,\ 0.99,\ 0.999,\ 0.9999,\ 0.99999,\ 0.999999$ from which we observe that the condition number increases as a gets closer to 1. We note that, in practice, if a vertex is very close to the interface, then we can treat it as an interface vertex.

Because of (2.4), these IFE shape functions are linearly independent. Hence, we can use them to define the local IFE space on each element $T \in \mathcal{T}_h$:

$$\mathcal{S}_h^{(p)}(T) = \begin{cases} Span\{L_i^{(p)}, i = 1, 2, \ldots, dim(\mathcal{P}_p)\}, & \forall T \in \mathcal{T}_h^n, \\ Span\{\varphi_i^{(p)}, i = 1, 2, \ldots, dim(\mathcal{P}_p)\}, & \forall T \in \mathcal{T}_h^i. \end{cases}$$

Of course, these local IFE spaces can be employed to construct pth degree IFE spaces $\mathcal{S}_h^p(\Omega), p \geq 1$ needed over Ω for a finite element method through the standard procedure. For example, we can use the following pth degree IFE space for a discontinuous Galerkin scheme

$$\mathcal{S}_h^p(\Omega) = \{u \mid u|_T \in \mathcal{S}_h^{(p)}(T)\}.$$

For illustration, we demonstrate quadratic IFE shape functions constructed according to (2.4) and (2.5) in Figs. 2.4 and 2.5 on the triangle with vertices (1, 0), (0, 0), (0, 1) cut by a circular interface centered at the origin with radius $r = 0.51$ where $\Omega^+ = \{(x,y) \mid x^2 + y^2 - r^2 > 0\}$ as shown in Fig. 2.3 (left) and using $\beta^+ = 10$ and $\beta^- = 1$. We further present jumps of six quadratic IFE shape functions $[\phi_i^{(2)}](t)$ across $T \cap \Gamma$ versus t for the triangle T having vertices (0, 0), $(h, 0)$, and (h, h), $h = 0.01$ and cut by the interface $y = \delta(e^{4x} - e^{4\delta})/(e^{4h} - e^{4\delta})$ shown in Fig. 2.3 (right) using $\delta = 0.75h$, $\beta^+ = 10$, $\beta^- = 1$. Computational experiments show that the jump $[\varphi_i^{(p)}](t)$ of each pth degree IFE shape function vanishes at least at $p+1$ points on the interface $T \cap \Gamma$, see plots in Fig. 2.6 showing the jumps across the interface for all quadratic IFE shape functions. Also, we have observed that if no vertex is on the interface, these intersection points converge to Gauss–Legendre points mapped to the interface as the element size $h \to 0$.

2.2. Hierarchical type IFE shape functions

Next we consider high degree IFE shape functions constructed by a procedure similar to the standard procedure for hierarchical FE shape functions [25,26] starting from the three vertex shape functions, then adding edge shape functions for $p \geq 2$ and then interior shape functions for $p \geq 3$. We start from a space related with $\mathcal{S}_h^{(p)}(T)$ for $p = 2, 3, \ldots$:

$$\mathcal{R}_0^p = \{\phi,\ |\ \phi|_{T^+} \in \mathcal{P}_p,\ \phi|_{T^-} = 0,\ \text{satisfying (2.2}a\text{) and (2.2}b\text{)}\}. \tag{2.7}$$

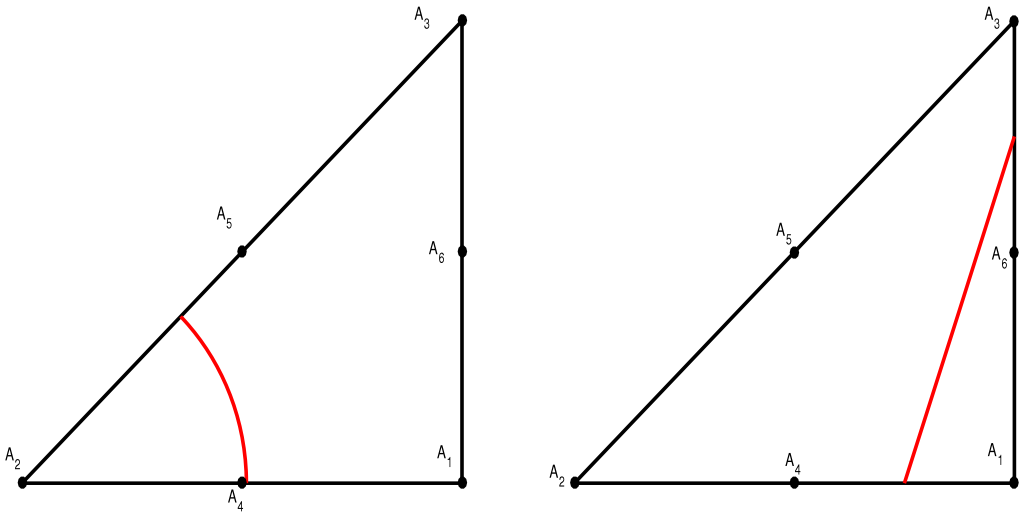

Fig. 2.3. Interface elements for quadratic IFE shape functions.

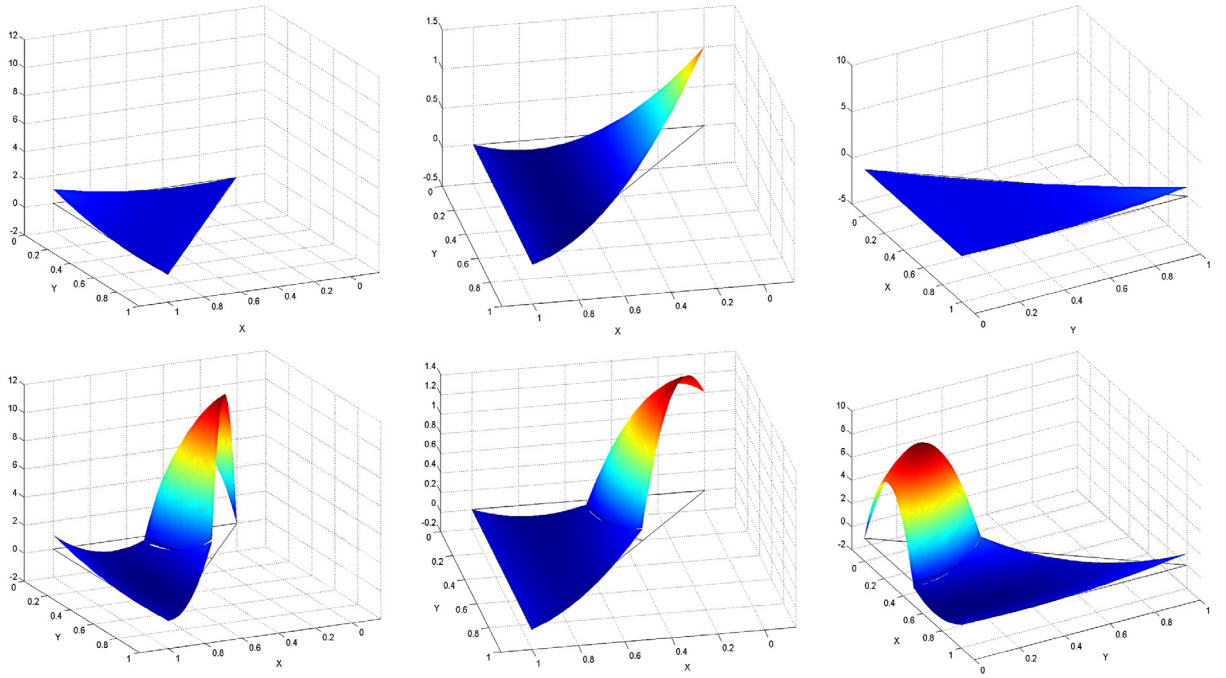

Fig. 2.4. Plots in the first row are quadratic vertex FE shape functions, those in the second row are their corresponding quadratic vertex IFE shape functions.

Note that $dim(\mathcal{R}_0^p) = dim(\mathcal{P}_p) - 2p - 1$. Each function $\psi^{(p)} \in \mathcal{R}_0^p$ can be written as

$$\psi^{(p)}|_{T^+} = \sum_{i=1}^{dim(\mathcal{P}_p)} c_i L_i^{(p)}. \tag{2.8}$$

Then, jump conditions (2.2a) and (2.2b) require its coefficients c_i, $1 \le i \le dim(\mathcal{P}_p)$ to satisfy a rectangular linear system $\mathbf{Ac} = 0$, where $\mathbf{c} = (c_1, c_2, \ldots, c_{dim(\mathcal{P}_p)})^t$. Let us now consider a basis of the null space of $\mathbf{A}$ as $\mathbf{c}^{(l)} = (c_1^{(l)}, c_2^{(l)}, \ldots, c_{dim(\mathcal{P}_p)}^{(l)})$, $l = 1, 2, \ldots, dim(\mathcal{R}_0^p)$ and use them to form basis functions $\psi_l^{(p)}$ in $\mathcal{R}_0^p$, $p \ge 2$ by

$$\psi_l^{(p)}(x, y) = \sum_{i=1}^{dim(\mathcal{P}_p)} c_i^{(l)} L_i^{(p)}(x, y), \quad l = 1, 2, \ldots, dim(\mathcal{R}_0^p). \tag{2.9}$$

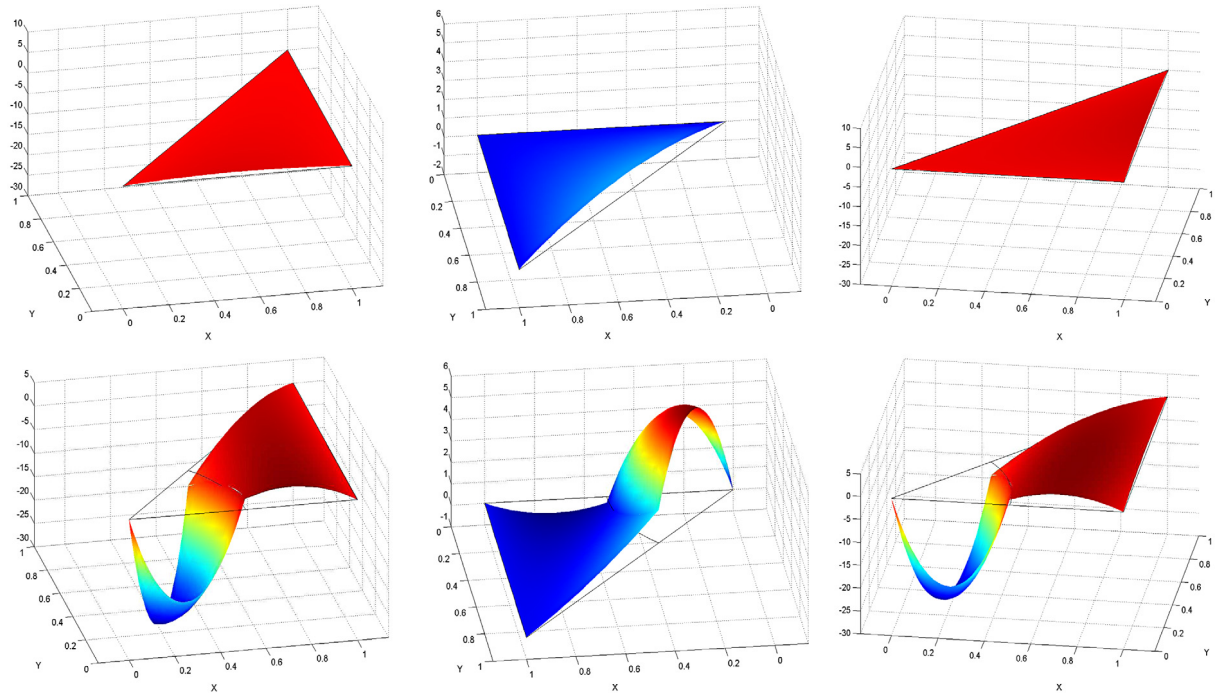

Fig. 2.5. Plots in the first row are quadratic edge FE shape functions, those in the second row are their corresponding quadratic edge IFE shape functions.

The procedure to construct hierarchical IFE shape functions for $S_h^{(p)}(T)$ is as follows:

- 3 vertex IFE shape functions

$$\varphi_i^{(1)}(x, y),\ i = 1, 2, 3, \tag{2.10}$$

  which are constructed according to (2.4) and (2.5).
- $3(p-1)$ (for $p \geq 2$) edge IFE shape functions

$$\varphi_i^{(k)} = \begin{cases} \varphi_i^{(1),+}(\varphi_j^{(1),+})^{k-1} + \sum_{l=1}^{dim(\mathcal{R}_0^k)} c_{l,k,i}\psi_l^{(k)}(x, y), & \text{on } T^+ \\ \varphi_i^{(1),-}(\varphi_j^{(1),-})^{k-1}, & \text{on } T^- \end{cases} \tag{2.11}$$

  for

$$k = 2, 3, \ldots, p, \text{ and } (i, j) = (1, 2), (2, 3), (3, 1).$$

  Here, subscript i in $\varphi_i^{(k)}$ emphasizes that $\varphi_i^{(k)}$ is associated with the ith edge of T.
- $(p-1)(p-2)/2$ (for $p \geq 3$) interior IFE shape functions

$$\varphi_{i,j}^{(k)} = \begin{cases} \varphi^{I,+}(\varphi_1^{(1),+})^i(\varphi_2^{(1),+})^j + \sum_{l=1}^{dim(\mathcal{R}_0^k)} c_{l,k,i,j}\psi_l^{(k)}(x, y), & \text{on } T^+ \\ \varphi^{I,-}(\varphi_1^{(1),-})^i(\varphi_2^{(1),-})^j, & \text{on } T^+ \end{cases} \tag{2.12}$$

  with $k = 3 + i + j$, $0 \leq i + j \leq p - 3$, and

$$\varphi^{I,\pm} = \varphi_1^{(1),\pm}\varphi_2^{(1),\pm}\varphi_3^{(1),\pm}. \tag{2.13}$$

Each edge IFE shape function $\varphi_i^{(k)}$ with $k \geq 2$ has $dim(\mathcal{R}_0^k)$ coefficients $c_{l,k,i}$ which are to be determined by applying the extended jump conditions (2.2c) with $p = k$ which lead to exactly $dim(\mathcal{R}_0^k)$ linear equations for $c_{l,k,i}$, $1 \leq l \leq dim(\mathcal{R}_0^k)$ for each i such that $1 \leq i \leq 3$. Similarly, for each (i, j) such that $0 \leq i + j \leq p - 3$, the coefficients of an interior IFE shape function $\varphi_{i,j}^{(k)}$ are also determined by applying the extended jump conditions (2.2c) with $p = k$ which lead to exactly $dim(\mathcal{R}_0^k)$ linear equations for $c_{l,k,i,j}$, $1 \leq l \leq dim(\mathcal{R}_0^k)$.

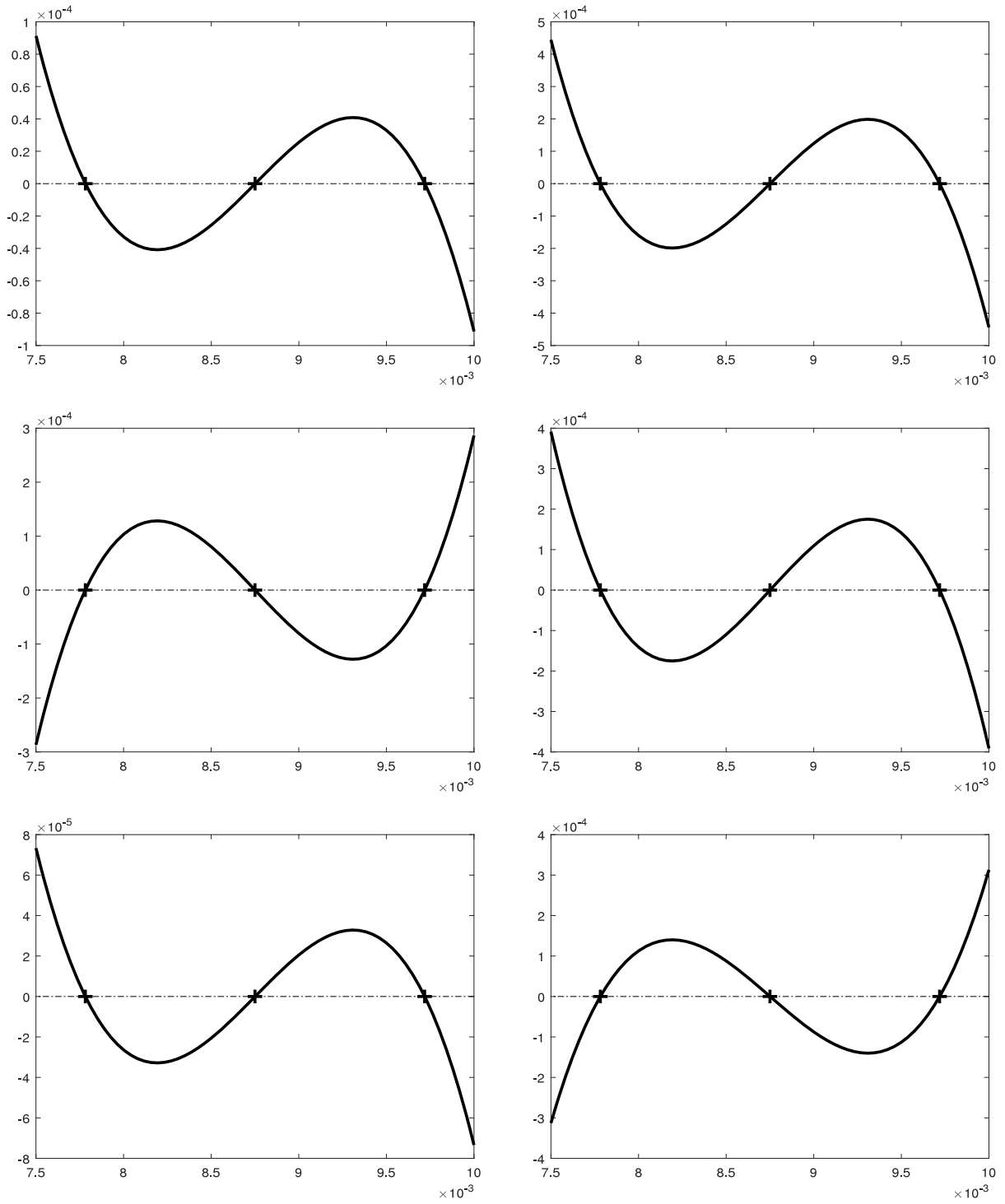

Fig. 2.6. Jumps of the quadratic IFE vertex (on the first column) and edge (on the second column) shape functions on the interface $T \cap \Gamma$. Legendre roots on the interface are marked by $+$.

On each interface element $T \in \mathcal{T}_h^i$, the local hierarchical IFE space $\mathcal{S}_h^{(p)}(T)$ is spanned by the vertex IFE shape functions given in (2.10), the edge IFE shape functions given in (2.11) when $p \geq 2$, and the interior IFE shape functions given in (2.12) when $p \geq 3$. Specifically, the local hierarchical IFE spaces up to $p = 5$ are given below:

$$\mathcal{S}_h^1(T) = Span\{\varphi_i^{(1)}, i = 1, 2, 3\},$$

$$\mathcal{S}_h^2(T) = Span\{\varphi_i^{(1)}, \varphi_i^{(2)}, i = 1, 2, 3\},$$
$$\mathcal{S}_h^3(T) = Span\{\varphi_i^{(1)}, \varphi_i^{(2)}, \varphi_i^{(3)}, 1 \le i \le 3, \varphi_{0,0}^{(3)}\},$$
$$\mathcal{S}_h^4(T) = Span\{\varphi_i^{(1)}, \varphi_i^{(2)}, \varphi_i^{(3)}, \varphi_i^{(4)}, 1 \le i \le 3, \varphi_{0,0}^{(3)}, \varphi_{1,0}^{(4)}, \varphi_{0,1}^{(4)}\},$$
$$\mathcal{S}_h^5(T) = Span\{\varphi_i^{(1)}, \varphi_i^{(2)}, \varphi_i^{(3)}, \varphi_i^{(4)}, \varphi_i^{(5)}, 1 \le i \le 3, \varphi_{0,0}^{(3)}, \varphi_{1,0}^{(4)}, \varphi_{0,1}^{(4)}, \varphi_{1,1}^{(5)}, \varphi_{2,0}^{(5)}, \varphi_{0,2}^{(5)}\}.$$

When $T \cap \Gamma$ is a straight line, we can verify that the vertex IFE shape functions $\varphi_i^{(1)}$, $1 \le i \le 3$ satisfy

$$[\varphi_i^{(1)}]_{T\cap\Gamma} = 0, \quad [\beta\, \boldsymbol{n} \cdot \nabla\varphi_i^{(1)}]_\Gamma = 0, \quad 1 \le i \le 3.$$

By [5], this further implies that, when $T \cap \Gamma$ is a straight line, the higher degree edge and interior hierarchical IFE shape functions and their normal fluxes satisfy the jump conditions (2.2a) and (2.2b), respectively. Because of this, for a general interface curve $T \cap \Gamma$, we expect these higher degree edge and interior IFE shape functions and their normal fluxes to satisfy the jump conditions (2.2a) and (2.2b) approximately when the mesh size h becomes small so that $T \cap \Gamma$ becomes very flat. The influence of this approximate satisfaction of interface jump conditions (2.2a) and (2.2b) on the performance of related IFE spaces constructed with these hierarchical IFE shape functions needs further investigation, our preliminary numerical experiments indicate that the proposed hierarchical higher degree IFE spaces can also perform optimally, see related examples presented in Section 4.

3. Some implementation issues

In this section, we discuss two key issues in applying higher degree IFE spaces for solving interface problems. The first one is about integrations on interface elements and the second is about suitable finite element schemes that can abate the impact of discontinuity of IFE functions across interface edges, which can be large for higher degree IFE functions.

Because higher degree IFE functions are piecewise polynomials defined on subelements T^- and T^+ formed by partitioning an interface element T with the actual curve $T \cap \Gamma$, integrations involving IFE functions have to be treated with care on interface elements. In principal, we should compute integrations on an interface element piecewisely on T^- and T^+. Furthermore, we note that computing an integral on a triangle with one curved edge can be carried out through the standard procedure by the change of variables that maps the curved triangle to the reference triangle where the integral value can be found by a preferred quadrature rule, see the left illustration in Fig. 3.1. Therefore, we suggest to partition T into smaller curved triangles, each of them is a subset of T^- or T^+, and carry out the integration through these curved triangles one by one.

In general, without loss of generality, when the mesh is fine enough we can assume that the interface $T \cap \Gamma$ generates two types of partitions of T: (i) the interface cuts the element T into 2 curved triangles; (ii) the interface cuts the element T into a curved triangle and a curved quadrilateral. As the illustration on the right in Fig. 3.1, the interface element $T = \triangle V_1V_2V_2$ is split by $T \cap \Gamma$ into a triangular region V_1DE with one curved edge $\widehat{DE} = T \cap \Gamma$ and a quadrilateral region EDV_2V_3 with the same curved edge $\widehat{ED} = T \cap \Gamma$. Then, the integration of u on T can be done by

$$\iint_T u dA = \iint_{V_1DE} u dA + \iint_{EDV_2V_3} u dA. \tag{3.1}$$

We then further divide the quadrilateral region EDV_2V_3 into $2m$ triangles each of which has one curved edge as follows. We assume that $T \cap \Gamma$ is parameterized by $(x(t), y(t))$, for $a \le t \le b$ and letting $(x(a), y(a)) = E$ and $(x(b), y(b)) = D$. We subdivide $[a, b]$ by $t_i = a + i\,dt$, $i = 1, 2, \ldots, m + 1$ with $dt = (b - a)/m$ and introduce the following points on $T \cap \Gamma$ by

$$Q_i = (x(t_i), y(t_i)), \ i = 1, 2, \ldots, m + 1, \tag{3.2}$$

and the points on the edge V_3V_2

$$P_i = V3\frac{(t_i - b)}{(a - b)} + V2\frac{(t_i - a)}{(b - a)}, \ i = 1, 2, \ldots, m + 1. \tag{3.3}$$

We now use these points to partition EDV_2V_3 into $2m$ triangles

$$P_iP_{i+1}Q_i, \ P_{i+1}Q_{i+1}Q_i, \ i = 1, 2, \ldots, m. \tag{3.4}$$

Finally, we can evaluate the integral over T as

$$\iint_T u dA = \iint_{V_1DE} u dA + \sum_{i=1}^{m}[\iint_{P_iP_{i+1}Q_i} u dA + \iint_{P_{i+1}Q_{i+1}Q_i} u dA]. \tag{3.5}$$

The other issue is about inevitable discontinuity of IFE functions across element edges. First, by definition, edge discontinuity of IFE functions in a scheme based on a discontinuous Galerkin (DG) formulation is an essential fact. Recall that the standard pth degree H^1 finite element space on the solution domain Ω is defined by requiring each finite element

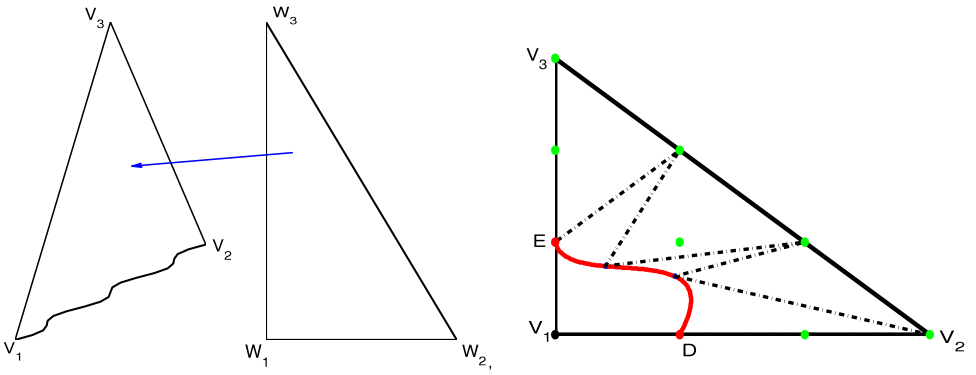

Fig. 3.1. The plot on the left is for the mapping between the reference triangle and a triangle with curved edge. The plot on the right is for the partition of an interface element for numerical quadrature.

function to be a pth degree polynomial when restricted on each element and by requiring each finite element function to be continuous at all Lagrange nodes in the mesh $\mathcal{T}_h$. When a standard pth degree H^1 finite element space is used in the Galerkin formulation, discontinuity is not a concern because all the finite element functions are continuous. However, even though each IFE function is defined such that its smoothness is maintained approximately across the interface Γ in each interface element, its continuity across every interface edge is not guaranteed because IFE shape functions on two of its adjacent elements are constructed according to different interface configurations such that they generally do not match on the common interface edge possibly except for the Lagrange nodes. Even if we require an IFE space on Ω to be continuous at all Lagrange nodes in the mesh, this IFE space is generally not a subspace of $H^1(\Omega)$, every IFE function in this space has discontinuity across the interface and interface edges but continuous everywhere else.

In the IFE spaces based on linear or bilinear polynomials with continuity at Lagrange nodes in the mesh, the discontinuity of IFE functions seems to be mild enough such that the usual Galerkin finite element scheme seems to work for the elliptic interface problem described by (1.1) and (1.2) albeit the involved bilinear form has to be defined as the sum of those locally defined on elements [10,14,15]. However, since higher degree polynomials are more oscillatory, the discontinuity in higher degree IFE functions are stronger so that, as observed in [5,7], the scheme based on the standard Galerkin formulation fails to perform optimally when used with higher degree IFE spaces. Nevertheless, we have observed that the penalty mechanism in standard discontinuous Galerkin (DG) methods [27–30] can be adopted to abate the discontinuity in IFE functions; hence, IFE methods based on DG formulations [31–33] for lower degree IFE spaces can be extended to higher degree IFE spaces. If a smaller number of global degrees of freedom is preferred, we can also use the Galerkin formulation plus penalty terms partially applied over interface edges [5,7,34].

4. Computational examples

We now present a few numerical examples to show the approximation capability of the pth degree IFE spaces. Consider the solution domain $\Omega = (0, 1)^2$ with the interface curve

$$\Gamma = \{(x, y) \mid (x - x_0)^2 + (y - y_0)^2 = r^2\} \tag{4.1}$$

where $(x_0, y_0) = (0.519, 0.613)$ and $r = 0.3317$, such that

$$\Omega^- = \{(x, y) \in \Omega \mid (x - x_0)^2 + (y - y_0)^2 < r^2\},$$
$$\Omega^+ = \{(x, y) \in \Omega \mid (x - x_0)^2 + (y - y_0)^2 > r^2\}.$$

The function $u(x, y)$ used in our numerical examples is

$$u(x, y) = \begin{cases} \dfrac{((x - x_0)^2 + (y - y_0)^2 - r^2)e^{6x+3y}}{\beta^+}, & (x, y) \in \Omega^+, \\ \dfrac{((x - x_0)^2 + (y - y_0)^2 - r^2)e^{6x+3y}}{\beta^-}, & (x, y) \in \Omega^-. \end{cases} \tag{4.2}$$

It can be verified that $u(x, y)$ satisfies the interface conditions in (1.2).

In each of the numerical examples to be presented, we use a uniform triangular mesh $\mathcal{T}_h$ obtained by partitioning Ω into $N \times N$ uniform squares and joining the lower-left and upper-right vertices of every square to form triangular elements in this mesh.

The convergence of the pth degree IFE interpolation: In this group of numerical examples, we demonstrate the approximation capability of pth degree IFE spaces by observing how fast the IFE interpolation can converge to a given function. All

Table 4.1
Interpolation errors for the IFE space with $p = 1$, $\beta^+ = 5$, $\beta^- = 1$.

N	$\|u - I_h u\|_0$	Order	$\|u_x - (I_h u)_x\|_{0,h}$	Order	$\|u_y - (I_h u)_y\|_{0,h}$	Order
20	1.3934	NA	7.4155e+01	NA	4.7436e+01	NA
30	6.2524e−01	1.9764	4.9851e+01	0.97942	3.1911e+01	0.97772
40	3.5318e−01	1.9854	3.7556e+01	0.98440	2.4001e+01	0.99017
50	2.2662e−01	1.9885	3.0100e+01	0.99177	1.9253e+01	0.98781
60	1.5768e−01	1.9893	2.5128e+01	0.99021	1.6061e+01	0.99428
70	1.1597e−01	1.9932	2.1554e+01	0.99543	1.3785e+01	0.99126
γ	NA	1.9848	NA	0.98639	NA	0.98696

Table 4.2
Interpolation errors for the IFE space with $p = 2$, $\beta^+ = 5$, $\beta^- = 1$.

N	$\|u - I_h u\|_0$	Order	$\|u_x - (I_h u)_x\|_{0,h}$	Order	$\|u_y - (I_h u)_y\|_{0,h}$	Order
20	4.7261e−02	NA	5.6566	NA	3.4196e+00	NA
30	1.4076e−02	2.9872	2.5471	1.9678	1.5427e+00	1.9632
40	6.0039e−03	2.9619	1.4482	1.9628	8.7377e−01	1.9760
50	3.0731e−03	3.0014	9.2918e−01	1.9886	5.6067e−01	1.9883
60	1.7945e−03	2.9504	6.4829e−01	1.9744	3.9067e−01	1.9815
70	1.1299e−03	3.0011	4.7665e−01	1.9951	2.8737e−01	1.9920
γ	NA	2.9788	NA	1.9741	NA	1.9773

Table 4.3
Interpolation errors for the IFE space with $p = 3$, $\beta^+ = 5$, $\beta^- = 1$.

N	$\|u - I_h u\|_0$	Order	$\|u_x - (I_h u)_x\|_{0,h}$	Order	$\|u_y - (I_h u)_y\|_{0,h}$	Order
20	1.5353e−03	NA	2.8786e−01	NA	1.7275e−01	NA
30	3.0613e−04	3.9768	8.5911e−02	2.9822	5.1555e−02	2.9822
40	9.7311e−05	3.9839	3.6403e−02	2.9848	2.1782e−02	2.9949
50	3.9922e−05	3.9929	1.8672e−02	2.9920	1.1144e−02	3.0033
60	1.9312e−05	3.9830	1.0830e−02	2.9875	6.4710e−03	2.9814
70	1.0432e−05	3.9949	6.8241e−03	2.9962	4.0793e−03	2.9932
γ	NA	3.9847	NA	2.9869	NA	2.9912

Table 4.4
Interpolation errors for the IFE space with $p = 4$, $\beta^+ = 5$, $\beta^- = 1$.

N	$\|u - I_h u\|_0$	Order	$\|u_x - (I_h u)_x\|_{0,h}$	Order	$\|u_y - (I_h u)_y\|_{0,h}$	Order
20	4.3251e−05	NA	1.1024e−02	NA	6.7607e−03	NA
30	5.7539e−06	4.9749	2.2007e−03	3.9739	1.3560e−03	3.9624
40	1.3700e−06	4.9884	6.9621e−04	4.0005	4.3184e−04	3.9773
50	4.4966e−07	4.9927	2.8577e−04	3.9906	1.7657e−04	4.0079
60	1.8030e−07	5.0123	1.3785e−04	3.9984	8.4291e−05	4.0558
70	8.3370e−08	5.0040	7.4518e−05	3.9906	4.5226e−05	4.0389
γ	NA	4.9904	NA	3.9900	NA	3.9965

related computations are done with the Lagrange type pth degree IFE space $S_h^p(\Omega)$, $p \geq 1$ defined in Section 2.1 with the requirement that each IFE function in $S_h^p(\Omega)$ is continuous at the standard Lagrange nodes of $\mathcal{T}_h$.

For a continuous function u, we define its pth degree IFE interpolation locally on each element $T = \triangle \in \mathcal{T}_h$ as

$$I_{h,T}u(x,y) = \begin{cases} \sum_{i=1}^{dim(\mathcal{P}_p)} u(A_i) L_i^{(p)}(x,y) & \text{for } T \in \mathcal{T}_h^n, \\ \sum_{i=1}^{dim(\mathcal{P}_p)} u(A_i) \varphi_i^{(p)}(x,y) & \text{for } T \in \mathcal{T}_h^i, \end{cases}$$

where A_i, $1 \leq i \leq dim(\mathcal{P}_p)$ are the nodes on element T associated with the usual pth degree Lagrange finite element shape functions. The p-degree IFE interpolation of u over the whole domain Ω is the IFE function $I_h u(x,y)$ piecewisely defined such that $I_h u|_T = I_{h,T}u$ for all $T \in \mathcal{T}_h$.

Tables 4.1–4.4 present errors of the pth degree IFE interpolation $I_h u$ for $p = 1, 2, 3, 4$ over a sequence of meshes for $N = 10, 20, \ldots, 70$. The values of γ in these tables are convergence rates $\mathcal{O}(h^\gamma)$ of the errors in $I_{h,T}u$ estimated by least-squares fitting of the data in these tables. The numerical data presented in Tables 4.1–4.4 clearly demonstrate that the pth degree IFE interpolation $I_h u$ converges to u optimally in both the L^2 and H^1 norms.

Table 4.5
Errors for the L^2 projection of the function (4.2) onto the hierarchical IFE space with $p = 2$, $\beta^+ = 5$, $\beta^- = 1$.

N	$\|u - I_h u\|_0$	Order	$\|u_x - (I_h u)_x\|_{0,h}$	Order	$\|u_y - (I_h u)_y\|_{0,h}$	Order
20	2.3000e−02	NA	4.7596e+00	NA	3.0604e+00	NA
30	7.0187e−03	2.9272	2.1955e+00	1.9084	1.4140e+00	1.9044
40	2.9897e−03	2.9665	1.2314e+00	2.0099	8.1171e−01	1.9293
50	1.5647e−03	2.9018	8.1069e−01	1.8735	5.3507e−01	1.8676
60	9.1271e−04	2.9563	5.6198e−01	2.0098	3.7970e−01	1.8814
70	5.8476e−04	2.8881	4.2425e−01	1.8238	2.8330e−01	1.9000
γ	NA	2.9340	NA	1.9378	NA	1.8993

Table 4.6
Errors for the L^2 projection of the function (4.3) onto the hierarchical IFE space with $p = 2$, $\beta^+ = 5$, $\beta^- = 1$.

N	$\|u - I_h u\|_0$	Order	$\|u_x - (I_h u)_x\|_{0,h}$	Order	$\|u_y - (I_h u)_y\|_{0,h}$	Order
20	3.0702e−02	NA	6.2889e+00	NA	4.3696e+00	NA
30	9.2362e−03	2.9626	2.8323e+00	1.9673	1.9690e+00	1.9660
40	3.9118e−03	2.9864	1.5992e+00	1.9869	1.1131e+00	1.9827
50	2.0109e−03	2.9820	1.0272e+00	1.9837	7.1553e−01	1.9801
60	1.1669e−03	2.9851	7.1505e−01	1.9868	4.9820e−01	1.9856
70	7.3557e−04	2.9934	5.2587e−01	1.9936	3.6653e−01	1.9911
γ	NA	2.9792	NA	1.9814	NA	1.9786

Table 4.7
IFE solution errors for $p = 1$, $\beta^+ = 5$, $\beta^- = 1$.

N	$\|u - U^h\|_0$	Order	$\|u_x - U^h_x\|_{0,h}$	Order	$\|u_y - U^h_y\|_{0,h}$	Order
20	1.2663	NA	7.4009e+01	NA	4.7275e+01	NA
30	5.7366e−01	1.9529	4.9767e+01	0.97870	3.1837e+01	0.97502
40	3.2170e−01	2.0107	3.7523e+01	0.98160	2.3966e+01	0.98729
50	2.0781e−01	1.9584	3.0071e+01	0.99213	1.9231e+01	0.98643
60	1.4372e−01	2.0226	2.5113e+01	0.98821	1.6046e+01	0.99300
70	1.0622e−01	1.9610	2.1539e+01	0.99594	1.3775e+01	0.99012
γ	NA	1.9813	NA	0.9852	NA	0.9848

The convergence of the L^2 projection to the hierarchical p-degree IFE spaces: Here we show approximation capability of the hierarchical IFE shape functions by the L^2 projection. For the function u defined by (4.2), we generate its piecewise L^2 projection on the Cartesian meshes used in the previous example. The errors in the L^2 projections of u and their rates of convergence are given in Table 4.5 from which we observe a near optimal convergence of the L^2 projections of u to the hierarchical quadratic IFE space.

We repeat the previous experiment for another function

$$u(x,y) = \begin{cases} \dfrac{(y + 0.871x - 1.337)e^{6x+3y}}{\beta^+}, & (x,y) \in \Omega^+, \\ \dfrac{(y + 0.871x - 1.337)e^{6x+3y}}{\beta^-}, & (x,y) \in \Omega^- \end{cases} \tag{4.3}$$

defined by a linear interface such that $\Omega^+ = \{(x,y) \,|\, y + 0.871x - 1.337 > 0\}$ and $\Omega^- = \{(x,y) \,|\, y + 0.871x - 1.337 < 0\}$. The errors in the L^2 projections of u and their rates of convergence are given in Table 4.6 that suggest an optimal approximation capability of the hierarchical quadratic IFE space.

The convergence of the p-degree IFE solution to the interface problem: This group of numerical results are for observing the convergence of the pth degree IFE solution $U_h \in S_h^p(\Omega)$ generated by the Galerkin method with the non-symmetric interior penalty partially applied over interface edges. The IFE spaces $S_h^p(\Omega)$, $p \geq 1$ used here are the Lagrange type with the requirement that each IFE function in $S_h^p(\Omega)$ is continuous at the standard Lagrange nodes of $\mathcal{T}_h$. The specific scheme is described in details in [5,34] with, of course, the substitution of the IFE spaces involved. The elliptic interface problem solved by this partially penalized pth degree IFE method is described by (1.1), (1.2a) and (1.2b) in which f and g chosen such that $u(x,y)$ given in (4.2) is the exact solution.

The errors of the pth degree IFE solution $U_h \in S_h^p(\Omega)$ are presented in Tables 4.7–4.10 for $p = 1, 2, 3, 4$ on a sequence of meshes with $N = 10, 20, \ldots, 70$. Again, the convergence rates γ estimated from the data in these tables indicate the optimal convergence of the pth degree IFE solution, in both the L^2 and H^1 norms.

In our numerical experiments, we have observed that the proposed higher degree IFE spaces also work well for elliptic interface problems whose diffusion coefficient β has a large discontinuity. Table 4.11 presents some typical data for the errors in the IFE solution produced in the proposed pth degree IFE spaces which clearly demonstrate the optimal convergence of the pth degree IFE solution to the interface problem whose coefficient has a quite large discontinuity.

Table 4.8
IFE solution errors for $p = 2$, $\beta^+ = 5$, $\beta^- = 1$.

N	$\|u - U^h\|_0$	Order	$\|u_x - U^h_x\|_{0,h}$	Order	$\|u_y - U^h_y\|_{0,h}$	Order
20	4.7261e−02	NA	5.6566	NA	3.4196	NA
30	1.4076e−02	2.9872	2.5471	1.9678	1.5427	1.9632
40	6.0039e−03	2.9619	1.4482	1.9628	8.7377e−01	1.9760
50	3.0731e−03	3.0014	9.2918e−01	1.9886	5.6067e−01	1.9883
60	1.7945e−03	2.9504	6.4829e−01	1.9744	3.9067e−01	1.9815
70	1.1299e−03	3.0011	4.7665e−01	1.9951	2.8737e−01	1.9920
γ	NA	2.9788	NA	1.9741	NA	1.9773

Table 4.9
IFE solution errors for $p = 3$, $\beta^+ = 5$, $\beta^- = 1$.

N	$\|u - U^h\|_0$	Order	$\|u_x - U^h_x\|_{0,h}$	Order	$\|u_y - U^h_y\|_{0,h}$	Order
20	1.4809e−03	NA	2.4962e−01	NA	1.5359e−01	NA
30	2.9168e−04	4.0071	7.4274e−02	2.9896	4.5660e−02	2.9918
40	9.1728e−05	4.0212	3.1454e−02	2.9868	1.9320e−02	2.9897
50	3.7570e−05	4.0002	1.6119e−02	2.9960	9.8902e−03	3.0008
60	1.8094e−05	4.0074	9.3470e−03	2.9888	5.7383e−03	2.9859
70	9.7594e−06	4.0049	5.8857e−03	3.0006	3.6130e−03	3.0011
γ	NA	4.0094	NA	2.9909	NA	2.9930

Table 4.10
IFE solution errors for $p = 4$, $\beta^+ = 5$, $\beta^- = 1$.

N	$\|u - U^h\|_0$	Order	$\|u_x - U^h_x\|_{0,h}$	Order	$\|u_y - U^h_y\|_{0,h}$	Order
20	4.2779e−05	4.9418	8.4800e−03	3.9593	5.2495e−03	3.9484
30	5.7400e−06	4.9538	1.6971e−03	3.9677	1.0517e−03	3.9651
40	1.3693e−06	4.9818	5.4001e−04	3.9804	3.3563e−04	3.9702
50	4.5115e−07	4.9755	2.2205e−04	3.9827	1.3804e−04	3.9817
60	1.8154e−07	4.9929	1.0740e−04	3.9839	6.6858e−05	3.9763
70	8.4186e−08	4.9851	5.8069e−05	3.9889	3.6101e−05	3.9977
γ	NA	4.9747	NA	3.9786	NA	3.9743

Table 4.11
IFE solution errors for $p = 4$, $\beta^+ = 10^3$, $\beta^- = 1$.

N	$\|u - U^h\|_0$	Order	$\|u_x - U^h_x\|_{0,h}$	Order	$\|u_y - U^h_y\|_{0,h}$	Order
20	2.2424e−05	NA	4.3058e−03	NA	2.8853e−03	NA
30	2.9834e−06	4.9747	8.7691e−04	3.9247	5.6871e−04	4.0053
40	7.4334e−07	4.8306	2.8895e−04	3.8590	1.8888e−04	3.8315
50	2.4392e−07	4.9937	1.1917e−04	3.9693	7.6582e−05	4.0456
60	9.9343e−08	4.9268	5.8201e−05	3.9305	3.7429e−05	3.9266
70	4.6246e−08	4.9601	3.1603e−05	3.9614	2.0249e−05	3.9854
γ	NA	4.9304	NA	3.9199	NA	3.9525

5. Conclusion

We have presented two procedures for constructing higher degree IFE shape functions with weakly imposed jump conditions across the actual interface. The higher degree IFE spaces have optimal approximation capability as demonstrated numerically with the convergence of the interpolation in these IFE spaces. The partially penalized pth degree IFE method also shows optimal convergence. Many challenges remain to be addressed such as related error analysis and the extension to systems of partial differential equations including interface problems for hyperbolic systems and Stokes problem.

Acknowledgment

This research was partially supported by the National Science Foundation (Grant Number DMS 1016313).

References

[1] I. Babuska, J.E. Osborn, Can a finite element method perform arbitrarily badly? Math. Comp. 69 (230) (2000) 443–462.
[2] J.H. Bramble, J.T. King, A finite element method for interface problems in domains with smooth boundary and interfaces, Adv. Comput. Math. 6 (1996) 109–138.
[3] Z. Chen, J. Zou, Finite element methods and their convergence for elliptic and parabolic interface problems, Numer. Math. 79 (1998) 175–202.
[4] S. Adjerid, T. Lin, Higher-order immersed discontinuous Galerkin methods, Int. J. Inf. Syst. Sci. 3 (2007) 558–565.

[5] S. Adjerid, M. Ben Romdhane, T. Lin, High-order interior penalty immersed finite element method for second-order elliptic interface problems, Int. J. Numer. Anal. Model. 11 (3) (2014) 541–566.
[6] S. Adjerid, T. Lin, A p^{th}-degree immersed finite element method for boundary value problems with discontinuous coefficients, Appl. Numer. Math. 59 (2009) 1303–1321.
[7] M. Ben-Romdhane, Higher-Degree Immersed Finite Elements for Second-Order Elliptic Interface Problems, Virginia Polytechnic Institute and State University, 2011 (Ph.D. thesis).
[8] B. Camp, T. Lin, Y. Lin, W.-W. Sun, Quadratic immersed finite element spaces and their approximation capabilities, Adv. Comput. Math. 24 (2006) 81–112.
[9] Y. Gong, B. Li, Z. Li, Immersed-interface finite-element methods for elliptic interface problems with non-homogeneous jump conditions, SIAM J. Numer. Anal. 46 (2008) 472–495.
[10] X. He, T. Lin, Y. Lin, Approximation capability of a bilinear immersed finite element space, Numer. Methods Partial Differential Equations 24 (2008) 1265–1300.
[11] X. He, T. Lin, Y. Lin, X. Zhang, Immersed finite element methods for parabolic equations with moving interface, Numer. Methods Partial Differential Equations 29 (2) (2013) 619–646.
[12] R. Kafafy, T. Lin, Y. Lin, J. Wang, 3-D immersed finite element methods for electric field simulation in composite materials, Internat. J. Numer. Methods Engrg. 64 (2005) 904–972.
[13] Z. Li, The immersed interface method using a finite element formulation, Appl. Numer. Math. 27 (1998) 253–267.
[14] Z. Li, T. Lin, X. Wu, New Cartesian grid methods for interface problems using finite element formulation, Numer. Math. 96 (1) (2003) 61–98.
[15] Z. Li, T. Lin, Y. Lin, R. Rogers, An immersed finite element space and its approximation capability, Numer. Methods Partial Differential Equations 20 (3) (2004) 338–367.
[16] T. Lin, Y. Lin, W.-W. Sun, Immersed finite element methods for 4th order differential equations, J. Comput. Appl. Math. 235 (13) (2011) 3953–3964.
[17] T. Lin, D. Sheen, X. Zhang, A locking-free immersed finite element method for planar elasticity interface problems, J. Comput. Phys. 274 (2013) 228–247.
[18] S.A. Suater, R. Warnke, Composite finite elements for elliptic boudnary value problems with discontinuous coefficients, Computing 77 (2006) 29–55.
[19] Sylvain Vallaghé, Théodore Papadopoulo, A trilinear immersed finite element method for solving the electroencephalography forward problem, SIAM J. Sci. Comput. 32 (2010) 2379–2394.
[20] D. Braess, Finite Elements: Theory, Fast Solvers, and Applications in Solid Mechanics, Cambridge University Press, New York, 2007.
[21] R.W. Clough, J.L. Tocher, Finite element stiffness matrices for analysis of plates in bending, in: J.R. Prezemieniecki, et al. (Eds.), Matrix Methods in Structual Mechanics, The Proceedings of the Conference held at Wright-Parrterson Air Force Base, Ohio, 26–28, October 1965, U.S. Department of Commerce, Virginia, 1966, pp. 515–545 National Technical Information Service.
[22] I. Babuska, J.E. Osborn, Generalized finite element methods: their performance and relation to mixed methods, SIAM J. Numer. Anal. 20 (3) (1983) 510–536.
[23] I. Babuska, J.E. Osborn, Finite element methods for the solution of problems with rough input data, in: P. Grisvard, W. Wendland, J.R. Whiteman (Eds.), Singular and Constructive Methods for their Treatment, in: Lecture Notes in Mathematics, vol. #1121, Springer-Verlag, New York, 1985, pp. 1–18.
[24] S. Adjerid, K. Moon, A higher order immersed discontinuous galerkin finite element method for the acoustic interface problem, in: A.R. Ansari (Ed.), Advances in Applied Mathematics, in: Springer Proceedings in Mathematics & Statistics, vol. 87, 2014, pp. 57–69.
[25] S. Adjerid, M. Aiffa, J.E. Flaherty, Hierarchical finite element bases for triangular and tetrahedral elements, Comput. Methods Appl. Mech. Engrg. 190 (1999) 2925–2941.
[26] B. Szabo, I. Babuska, Finite Element Analysis, John Wiley, New York, 1991.
[27] D.N. Arnold, F. Brezzi, B. Cockburn, L.D. Marini, Unified analysis of discontinuous galerkin methods for elliptic problems, SIAM J. Numer. Anal. 39 (2000) 1749–1779.
[28] J.T. Oden, Ivo Babuska, C.E. Baumann, A discontinuous hp finite element method for diffusion problems, J. Comput. Phys. 146 (1998) 491–519.
[29] Beatrice Rivière, Discontinuous Galerkin Methods for Solving Elliptic and Parabolic Equations, in: Frontiers in Applied Mathematics, SIAM, Philadelphia, 2008.
[30] B. Riviere, M.F. Wheeler, V. Giraut, Improved energy estimates for finite elements methods based on discontinuous approximations spaces for elliptic problems, SIAM J. Numer. Anal. 39 (2001) 902–931.
[31] X. He, T. Lin, Y. Lin, Interior penalty bilinear IFE discontinuous Galerkin methods for elliptic equations with discontinuous coefficient, J. Syst. Sci. Complex. 23 (2010) 467–483.
[32] X. He, T. Lin, Y. Lin, A selective immersed discontinuous Galerkin method for elliptic interface problems, Math. Methods Appl. Sci. 37 (7) (2013) 938–1002.
[33] Tao Lin, Qing Yang, Xu Zhang, A priori error estimates for some discontinuous galerkin immersed finite element methods, J. Sci. Comput. 65 (2015) 875–894.
[34] Tao Lin, Yanping Lin, Xu Zhang, Partially penalized immersed finite element methods for elliptic interface problems, SIAM J. Numer. Anal. 53 (2015) 1121–1141.